Reconfigurable Intelligent Surface-Empowered Code Index Modulation for High-Rate SISO Systems

Fatih Cogen, Burak Ahmet Ozden, Erdogan Aydin, and Nihat Kabaoglu

***Abstract*—In this study, a novel index modulation-based communication system is proposed by combining the recently popular code index modulation-spread spectrum (CIM-SS) and reconfigurable intelligent surface (RIS) techniques. This technique is called CIM-RIS in short. In this proposed system, in addition to the traditional modulated symbols, the spreading code indices also carry data by being embedded in the signal, and the reflection/scattering properties of the signals are voluntarily controlled via the RIS technique. Consequently, the proposed system consumes little energy while transmitting extra bits of information compared to the traditional RIS. Average bit-error error (ABER) analysis of the proposed system is carried out and the system complexity, energy efficiency, and throughput analyses are obtained. The capacity analysis of the proposed CIM-RIS system is derived and it is shown that it provides higher capacity than the RIS-RSM and RIS systems. Performance analysis of the system is carried out on both Rayleigh fading channels and Rician fading channels for the *M*-ary quadrature amplitude modulation (QAM) technique. It has been shown by computer simulations that the CIM-RIS scheme has better error performance, faster data transmission speed, and lower transmission energy, compared to traditional RIS, transmit spatial modulation aided RIS (TSM-RIS), and transmit quadrature spatial modulation-based RIS (TQSM-RIS) techniques. In addition, the performance of the proposed system under conditions of imperfect channel state information (CSI) has also been obtained and illustrated.**

***Index Terms*—Index modulation, reconfigurable intelligent surface, code index modulation, energy efficiency, high data-rate.**

I. Introduction

In RECENT years, in addition to Internet applications like heavy data use, online-gaming, and streaming high-definition video; several Internet of Things (IoT) industries have emerged, including wearable technology, smart home appliances, audiovisual devices, smart measurement, and fleet management. High data rates and energy efficiency are unquestionably needed in these sectors since they have emerged as two of the most pressing problems of our day [1], [2]. It is a fact that by 2025, there will be close to 80 million Internet-connected gadgets. This viewpoint makes it clear that the next generation of communication methods should be high data-rated and energy-efficient [3], [4], [5].

Rational communication techniques such as index modulation (IM) are among the topics that have been frequently emphasized in recent years, as the advances in new technologies are increasing rapidly and existing users expect better, more efficient, and versatile services [4]. In IM, the indices of the units such as the transmitter antenna, subcarrier, time interval, spreading code, precoding matrix are taken into consideration for the transmission of information. In this telecommunication technique, extra information is ferried together with the transmitted or received signals in the form of indices that are embedded in the signals [6], [7], [8]. Therefore, little to no effort is put towards carrying more information in indices. As a result, energy efficiency is increased along with spectral efficiency thanks to IM [6], [7]. Code index modulation (CIM) system, which is based on IM technique and is one of the building blocks of this publication, uses the indices of the Walsh Hadamard spreading codes to carry extra information in addition to the symbols that are conveyed [3], [4], [5]. Specifically, it uses some of the data bits to modulate the symbol to be transmitted and another to select the spreading codes to be activated. Thus, additional information is loaded into the index of the spreading codes. Consequently, the CIM system boosts the communication system's energy-efficiency and data rate while lowering energy usage [5], [9], [10], [11].

Multiple-input multiple-output (MIMO) techniques considerably improve telecommunication system performance and are competitive options for next-generation wireless telecommunication systems [4]. The most important MIMO technique, which has recently emerged in the literature and has become the focus of research, is unquestionably the spatial modulation technique (SM) [12]. One of the members of the SM family, which has attracted more attention in recent years compared to SM, is undoubtedly the quadrature spatial modulation (QSM) technique. When compared to the SM approach, the QSM technique doubles the number of antennas, improving band efficiency. Since the QSM technique inherits all its other features from SM, inter-channel interferenc (ICI) and synchronization problems are not observed in QSM as in SM [3].

As a result of the concept of smart meta-surfaces, researchers have also lately concentrated on managing the propagation

Manuscript received 4 September 2023; revised 20 February 2024; accepted 23 March 2024. Date of publication 3 April 2024; date of current version 8 October 2024. This work was supported by The Scientific and Technological Research Council of Turkey (TUBITAK) through the 1515 Frontier Research and Development Laboratories Support Program under Project 5229901 - 6GEN. Lab: 6G and Artificial Intelligence Laboratory. Also, this work was supported by TUBITAK 1001 (Grant Number: 123E513). The associate editor coordinating the review of this article and approving it for publication was L. Liang. *(Corresponding author: Erdogan Aydin.)*

Fatih Cogen is with the Department of Electrical and Electronics Engineering, Istanbul Medeniyet University, 34857 Istanbul, Turkey, and also with the 6GEN. Lab, Turkcell Iletisim Hizmetleri Inc., 34854 Istanbul, Turkey (e-mail: fatih.cogen@turkcell.com.tr).

Burak Ahmet Ozden is with the Department of Computer Engineering, Yıldız Technical University (Davutpasa), 34220 Istanbul, Turkey, and also with the Department of Electrical and Electronics Engineering, Istanbul Medeniyet University, 34857 Istanbul, Turkey (e-mail: bozden@yildiz.edu.tr).

Erdogan Aydin and Nihat Kabaoglu are with the Department of Electrical and Electronics Engineering, Istanbul Medeniyet University, 34857 Istanbul, Turkey (e-mail: erdogan.aydin@medeniyet.edu.tr; nihat.kabaoglu@medeniyet.edu.tr).

Digital Object Identifier 10.1109/TCCN.2024.3384495

environment to increase spectrum efficiency and service quality [13]. To enhance the signal quality in the transmitter, thin films of electromagnetic and reconfigurable materials are placed in various environmental objects in the reconfigurable smart surface (RIS) structure. These materials are deliberately controlled by smart software [14]. Actually, there are many low cost and small passive elements in a RIS structure; through these elements, RIS just reflects the input signal with a phase shift that is adjustable. Since the performance of the reflective array elements in RIS does not decrease with the effects of self-interference and noise amplification, RIS is seen as a strong next-generation communication candidate [15], [16].

Studies in the field of RIS have been put forward to serve the same purpose with different names since 2012. Active frequency selective surfaces are used in [17] to control the signal coverage under the name of "transmission through smart walls". A communication technique including beamforming using passive reflective elements in [18] has been proposed. In studies number [13], [19], [20], the authors studied a downlink scenario with RIS support and focused on energy-efficiency and data rate maximization in this study. Also, in the same studies, the selection of optimum-RIS phases has been emphasized and low-complexity optimization schemes have been investigated for RIS. In [21] and [22], the common active and passive beam configuration problem is discussed and the average received power of the user is investigated. Physical layer security schemes of systems using RIS are mentioned in [23]. In [24], the average symbol error probability (SEP) statement is presented for RIS supported systems. RIS-based MIMO systems have been evaluated in [25], a low complexity algorithm based on the cosine-similarity theorem has been proposed to adapt phase shifts in [26], and in [27] RIS based space shift keying system has been proposed. In addition, the publications [28], [29], and [30], which contain general information in this area, can be reviewed by researchers who want to obtain large-scale information about RIS. In [31] a new high performance and high spectral efficiency RIS aided spatial media-based modulation system, shortly called RIS-SMBM, is presented. In [32], the focus is shifted from SM to metasurface-based modulation to implement single-RF MIMO. A comparison is conducted between antenna-based and metasurface-based modulation to underscore the advantages of utilizing metasurfaces. In [33], a reflecting modulation (RM) scheme for RIS-based communications is proposed, where information is conveyed through both reflecting patterns and transmit signals. In [34], passive beamforming and information transfer (PBIT) for multiuser MIMO systems are investigated, aided by RIS. Additionally, the PBIT design is extended from single-RIS to multi-RIS systems, leveraging similarities between the two. In [35], an investigation is presented on a system utilizing RIS for passive PBIT, with the focus being on optimizing beamforming strategies and assessing performance improvements through simulations. In [36], a cyclic-prefixed single-carrier (CPSC) transmission scheme integrated with PSK and empowered by a RIS is presented for enhancing broadband wireless communications. The RIS is utilized to create diverse cyclically delayed versions of the incident signal, aiming for multipath diversity in the proposed CPSC-RIS system.

A. Contributions

Based on the aforementioned needs in next-generation communication techniques, in this publication, combining the newly popular CIM-SS and RIS approaches, a unique communication system called CIM-RIS is presented. In this proposed system, the Walsh Hadamard spreading code indices carry data by being included into the signal in addition to the conventional modulated symbols, and the reflection/scattering properties of the signals are voluntarily controlled via the RIS.

The integration of CIM-SS with RIS technologies in the proposed CIM-RIS system is driven by the urgent need for more energy-efficient and high-capacity wireless communication systems. As the demand for ubiquitous connectivity and IoT applications grows exponentially, traditional communication systems face significant challenges in meeting the required data rates while maintaining low energy consumption and minimal interference. The innovative combination of CIM-SS and RIS in CIM-RIS addresses these challenges by leveraging the spatial dimension for data transmission, significantly enhancing the system's spectral and energy efficiency without increasing the hardware complexity. This approach not only promises substantial improvements in system performance but also aligns with the future direction of wireless networks, which necessitates intelligent and adaptive environments to cope with the ever-increasing data traffic and diverse communication requirements.

As a result of the analyzes and theoretical derivations, the contribution of the study can be given as follows:

1) Average bit-error rate (ABER), energy efficiency, complexity, and throughput analyzes are derived for the CIM-RIS scheme. All these analyzes are presented in comparison with RIS, transmit SM-RIS (TSM-RIS), and transmit QSM-RIS (TQSM-RIS) methods.
2) The capacity analysis of the CIM-RIS system has been obtained, and it has been compared with benchmark systems visually.
3) The performance of the system for the imperfect CSI case is also presented. This inclusion aims to realistically assess the system's robustness and adaptability in environments where channel conditions are uncertain or partially known.
4) Furthermore, the investigation has been extended to include the analysis of the proposed CIM-RIS system's performance under Rician fading channels. This analysis has been deemed crucial for understanding how the system behaves in scenarios where the line-of-sight component significantly influences the wireless communication environments.
5) The simulation results demonstrate that the proposed CIM-RIS technique has more performance than traditional RIS, TSM-RIS, and TQSM-RIS communication techniques. In addition, due to the nature of CIM, which is the building block of the CIM-RIS technique, it uses less energy than the systems discussed above.

B. Organization and Notations

We introduce the CIM-RIS system in Section II. Performance study of the CIM-RIS scheme is provided in

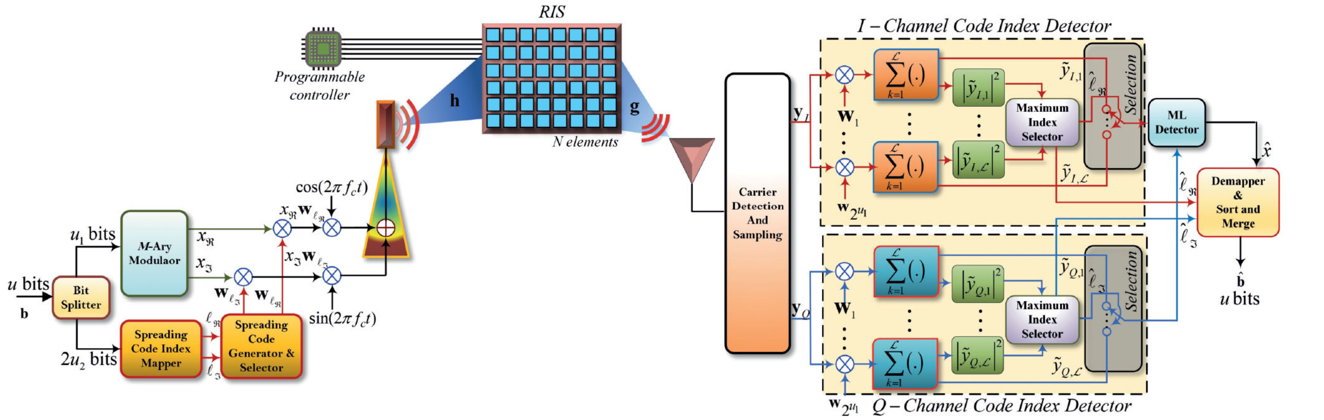

Fig. 1. The CIM-RIS technique's system model.

Section III. In Section IV the capacity analysis is conducted. Section V covers the analysis of complexity, throughput, energy efficiency, and data rate. Section VI includes the simulation results of the proposed scheme and the comparison of these results with the other systems mentioned. Finally, Section VII brings the paper to a close.

Notation: Bold lowercase and uppercase symbols denote matrices and vectors, respectively. The Hermitian, transposition, and Frobenius norm operators are denoted by $(\cdot)^H$, $(\cdot)^T$, and $\|\cdot\|_F$, $|\cdot|$, respectively. The real and imaginary components of a complex-valued quantity are denoted by $\Re(.)$ and $\Im(.)$. $\mathrm{E}[\,\cdot\,]$ and the $\mathrm{Var}[\,\cdot\,]$ are the expectation and the variance operators.

II. System Model

Fig. 1 shows the proposed CIM-RIS system model. In order to optimize the signal-to-noise ratio (SNR) at the destination terminal $(\mathcal{D})$, it is expected for the CIM-RIS approach that the RIS is managed by the source terminal $(\mathcal{S})$ with software that selects the reflection phases. This structure is also known as "smart RIS". There are N reconfigurable reflection elements in the structure of RIS. $h_{k,n}$ and $g_{k,n}$ used here are the channel fading coefficients between $\mathcal{S}$ – RIS and RIS $-\mathcal{D}$ of the n^{th} RIS element of the k^{th} chip, respectively, where $k \in \{1, 2, \ldots, K\}$ and $n \in \{1, 2, \ldots, N\}$. For the CIM-RIS technique, traditional M-QAM modulation has been considered to further improve spectral efficiency. In addition, in the system structure $\mathcal{L}$ spreading Walsh Hadamard codes $\mathbf{w}_\ell = [w_{\ell,1}, w_{\ell,2}, \ldots, w_{\ell,K}]^T$, $\ell \in \{1, 2, \ldots, \mathcal{L}\}$ are used, and each code consists of K chips.

If the transmitter terminal structure of the CIM-RIS system is properly analyzed, the binary information bits vector that will be sent during the τ_s symbol-period in this system is $\mathbf{b}$ with the size of $1 \times u$. $\mathbf{b}$ is split into two sub-vectors of $u_1 = \log_2(M)$ and $2u_2 = 2\log_2(\mathcal{L})$ bits in the CIM-RIS transmitter, where $u = u_1 + 2u_2$. The information is transferred from $\mathcal{S}$ to $\mathcal{D}$ through RIS after being selected in the transmitter by u_1 bits for the M-QAM symbol and $2u_2$ bits for the spreading code indices of the IQ-components.

The general form of the M-QAM modulated complex symbol is expressed as $x = x_\Re + jx_\Im$, where the real and imaginary parts of x, respectively, are denoted by $x_\Re$ and $x_\Im$. The bit sequence u_1 is used to determine the selection of $x_\Re$ and $x_\Im$. The $\mathbf{w}_{\ell_\Re}$ and $\mathbf{w}_{\ell_\Im}$ spreading codes, which are composed of $\pm\frac{1}{\sqrt{K}}$, spreaded the $x_\Re$ and $x_\Im$. These spreading codes are chosen based on the bits sequence of $2u_2$.

Based on the above mentioned information, the k^{th} chip signal obtained from RIS at $\mathcal{D}$ may be stated as follows:

$$y(t) = \sqrt{E_x}\sum_{k=1}^{K}\big(x_\Re\, w_{\ell_\Re,k}\, p(t-k\tau_c)\cos(2\pi f_c t) + x_\Im\, w_{\ell_\Im,k} \times p(t-k\tau_c)\sin(2\pi f_c t)\big)(h(t)*g(t))e^{\phi(t)} + n(t), \tag{1}$$

where, the unit rectangular pulse shaping filter with a time period of $[0, \tau_c]$ is called $p(t)$, The additive white Gaussian noise with N_0 variance and a mean of zero is known as $n(t)$, i.e., $\mathcal{CN}(0, N_0)$. The adjusting phase of the RIS is denoted by $\phi(t)$, the channel between $\mathcal{S}$ and RIS is "$h(t)$", while the channel between RIS and $\mathcal{D}$ is "$g(t)$".

The signal model provided in (1) may be rewritten separately for the IQ-components because they have a similar structure. As a result, the k^{th} noisy chip signal is delivered for the two IQ-components after the channel's output performs perfect carrier detection and sampling:

$$\begin{aligned} y_{I,k} &= \sqrt{E_{x_\Re}}\left(\sum_{n=1}^{N} h_{k,n}e^{j\phi_{k,n}}g_{k,n}\right)x_\Re\, w_{\ell_\Re,k} + n_{I,k} \\ &= \sqrt{E_{x_\Re}}\left(\sum_{n=1}^{N}\alpha_{k,n}\beta_{k,n}e^{j(\theta_{k,n}+\varphi_{k,n}-\phi_{k,n})}\right)x_\Re\, w_{\ell_\Re,k} \\ &\quad + n_{I,k} = \sqrt{E_{x_\Re}}\,\mathbf{h}_k^T\,\mathbf{\Phi}\,\mathbf{g}_k\, x_\Re\, w_{\ell_\Re,k} + n_{I,k}, \end{aligned} \tag{2}$$

$$\begin{aligned} y_{Q,k} &= \sqrt{E_{x_\Im}}\left(\sum_{n=1}^{N} h_{k,n}e^{j\phi_{k,n}}g_{k,n}\right)x_\Im\, w_{\ell_\Im,k} + n_{Q,k} \\ &= \sqrt{E_{x_\Im}}\left(\sum_{n=1}^{N}\alpha_{k,n}\beta_{k,n}e^{j(\theta_{k,n}+\varphi_{k,n}-\phi_{k,n})}\right)x_\Im\, w_{\ell_\Im,k} \\ &\quad + n_{Q,k} = \sqrt{E_{x_\Im}}\,\mathbf{h}_k^T\,\mathbf{\Phi}\,\mathbf{g}_k\, x_\Im\, w_{\ell_\Im,k} + n_{Q,k}, \end{aligned} \tag{3}$$

where, $E_{x_\Re}$ denotes the energy of the real component of the symbol and $E_{x_\Im}$ denotes the energy of the imaginary component of the symbol. Also, $h_{k,n}$ and $g_{k,n}$ are specified as $h_{k,n} = \alpha_{k,n}e^{-j\theta_{k,n}}$ and $g_{k,n} = \beta_n e^{-j\varphi_{k,n}}$ with zero mean and $\sigma_h^2 = \sigma_g^2 = \sigma^2$ variance, respectively, and both follow the Rayleigh fading channel. Here, $\mathbf{h}_k$ and $\mathbf{g}_k$ can be defined as respectively: $\mathbf{h}_k = [h_{k,1}, \ldots, h_{k,N}]^T$; $\mathbf{g}_k = [g_{k,1}, \ldots, g_{k,N}]^T$. $\mathbf{\Phi}$ is a reflection matrix (also known as a passive beamformer) that contains the reflection phases brought on by N reflecting components.

$\mathbf{\Phi}$ is controlled by the RIS control signal from the $\mathcal{S}$ and then, $\mathbf{\Phi} = \mathtt{diag}\{e^{j\phi_{k,1}}, e^{j\phi_{k,2}}, \ldots, e^{j\phi_{k,N}}\}$. As $\phi_k^n = (\theta_{\ell,k}^n + \varphi_n)$ for $n \in \{1, 2, \ldots, N\}$, the smart RIS $\mathbf{h}_k$ and $\mathbf{g}_k$. The noise term for the k^{th} chip of the I channel is $n_{I,k}$ and for the k^{th} chip of the Q channel is $n_{Q,k}$. Since $n_k = n_{I,k} + jn_{Q,k}$, the vector representation of the noisy received baseband signal in (2) and (3) may be represented as:

$$\mathbf{y}_I = \sqrt{E_{x_\Re}}\ \mathbf{h}^T\ \mathbf{\Phi}\ \mathbf{g}\ x_\Re\ \mathbf{w}_{\ell_\Re}^T + \mathbf{n}_I,$$
$$\mathbf{y}_Q = \sqrt{E_{x_\Im}}\ \mathbf{h}^T\ \mathbf{\Phi}\ \mathbf{g}\ x_\Im\ \mathbf{w}_{\ell_\Im}^T + \mathbf{n}_Q, \tag{4}$$

here, the vector expression of the noisy signals in *IQ*-channel received for $k = 1, 2, \ldots, K$ are $\mathbf{y}_I = [y_{I,1}, y_{I,2}, \ldots, y_{I,K}]^T$ and $\mathbf{y}_Q = [y_{Q,1}, y_{Q,2}, \ldots, y_{Q,K}]^T$, respectively. It is envisaged in the Smart RIS structure that a computer program will supply RIS with channel state information (CSI). Assuming that the channel does not change by the symbol time (flat-fading channel), i.e., $\mathbf{h}_1 = \mathbf{h}_2 = \ldots = \mathbf{h}_K$ and $\mathbf{g}_1 = \mathbf{g}_2 = \ldots = \mathbf{g}_K$ are $\mathbf{h}_k = [h_{k,1}, \ldots, h_{k,N}]^T$ and $\mathbf{g}_k = [g_{k,1}, \ldots, g_{k,N}]^T$. Therefore, the instantaneous total SNR at $\mathcal{D}$ in *I*-channel over a period $\tau_s = K\tau_c$ may be stated as follows:

$$\gamma = \frac{E_{x_\Re}\left|\left(\sum_{n=1}^N \alpha_{1,n}\beta_{1,n}\, e^{\left(j\phi_{1,n} - j\theta_{1,n} - j\varphi_{1,n}\right)}\right) w_{\ell,1}\right|^2}{N_0} + \\ \vdots \\ + \frac{E_{x_\Re}\left|\left(\sum_{n=1}^N \alpha_{K,n}\beta_{K,n}\, e^{\left(j\phi_{K,n} - j\theta_{K,n} - j\varphi_{K,n}\right)}\right) w_{\ell,K}\right|^2}{N_0} \tag{5}$$

here, it is clear that by eliminating channel phases, the value of γ can be maximized. That is to say, under the assumption that RIS knows the $\theta_{k,n}$ and $\varphi_{k,n}$ channel phases, SNR is maximized if $\phi_{k,n} = \theta_{k,n} + \varphi_{k,n}$. The maximum instantaneous SNR at $\mathcal{D}$ may be expressed as follows under the assumption of a flat-fading channel:

$$\gamma_{max} = \frac{E_{x_\Re}\left(\sum_{n=1}^N \alpha_n\beta_n\right)^2}{N_0}. \tag{6}$$

In $\mathcal{D}$, the baseband sampled signal is used to determine the Walsh Hadamard spreading code index first. As a result, the vectors $\mathbf{y}_I$ and $\mathbf{y}_Q$ are multiplied by the relevant $\mathbf{w}_i$ Walsh Hadamard spreading code through the associated receiver for *IQ*-components and added throughout the period of the $\tau_s = K\tau_c$ symbol as follows:

$$\begin{aligned}\tilde{y}_{I,\ell} &= \sum_{k=1}^K w_{\ell,k}\, y_{I,k} \\ &= \sum_{k=1}^K w_{\ell,k}\left(\sqrt{E_{x_\Re}}\left(\sum_{n=1}^N \alpha_n\beta_n\right) w_{\ell_\Re,k}x_\Re + n_{I,k}\right) \\ &= \begin{cases}\sqrt{E_{x_\Re}}\left(\sum_{n=1}^N \alpha_n\beta_n\right) x_\Re + \tilde{n}_I, & \text{if } \ell = \hat{\ell}_\Re \\ \tilde{n}_I, & \text{if } \ell \neq \hat{\ell}_\Re\end{cases}\end{aligned} \tag{7}$$

$$\begin{aligned}\tilde{y}_{Q,\ell} &= \sum_{k=1}^K w_{\ell,k}\, y_{Q,k} \\ &= \sum_{k=1}^K w_{\ell,k}\left(\sqrt{E_{x_\Im}}\left(\sum_{n=1}^N \alpha_n\beta_n\right) w_{\ell_\Im,k}x_\Im + n_{Q,k}\right) \\ &= \begin{cases}\sqrt{E_{x_\Im}}\left(\sum_{n=1}^N \alpha_n\beta_n\right) x_\Im + \tilde{n}_Q, & \text{if } \ell = \hat{\ell}_\Im \\ \tilde{n}_Q, & \text{if } \ell \neq \hat{\ell}_\Im\end{cases}\end{aligned} \tag{8}$$

where $\tilde{n}_I = \sum_{k=1}^K w_{\ell,k}n_{I,k}$ and $\tilde{n}_Q = \sum_{k=1}^K w_{\ell,k}n_{Q,k}$ are AWGN noise multiplied by the Walsh Hadamard code at the receiver. The resultant vector set at the receiver side may be described as follows when despreading process is carried out through every despreader for both *IQ*-components:

$$\mathcal{S}_I = \{\tilde{y}_{I,1}, \tilde{y}_{I,2}, \ldots, \tilde{y}_{I,\mathcal{L}}\}, \tag{9}$$
$$\mathcal{S}_Q = \{\tilde{y}_{Q,1}, \tilde{y}_{Q,2}, \ldots, \tilde{y}_{Q,\mathcal{L}}\}. \tag{10}$$

After despreading at the receiver terminal, as seen on the receiver side of Fig. 1, data $(\hat{\ell}_\Re, \hat{\ell}_\Im, \hat{x})$ –which represent estimates of the spreading code index and the transmitted symbol—are acquired. The code indexes $(\hat{\ell}_\Re, \hat{\ell}_\Im)$ is initially identified in order to lessen the complexity of the CIM-RIS system, and then $\hat{x}$ will then be estimated. In order to solely apply the $(\tilde{y}_{I,\hat{\ell}_\Re}, \tilde{y}_{Q,\hat{\ell}_\Im})$ despreading data linked with the $(\hat{\ell}_\Re, \hat{\ell}_\Im)$ to the input of the maximum likelihood estimator, the acquired $(\hat{\ell}_\Re, \hat{\ell}_\Im)$ index is then reported back to the despreading vector set. The system's complexity is significantly reduced in this way.

The absolute square of the elements in $\mathcal{S}_I$ and $\mathcal{S}_Q$ are computed first, followed by the estimation of the greatest element of the set's $\{|\tilde{y}_{I,\ell}|^2\}_{\ell=1}^{\mathcal{L}}$ and $\{|\tilde{y}_{Q,\ell}|^2\}_{\ell=1}^{\mathcal{L}}$ indexes to estimate the code index. Given that the spreading Walsh Hadamard spreading codes are orthogonal to one another, the normed vector's highest valued element corresponds to the despreaded element within the same index. i.e., $\sum_{k=1}^K w_{\iota,k}\, w_{\varpi,k} = 1$ if $\iota = \varpi; 0$ if $\iota \neq \varpi$.

As a result, the following code index detection method employs the index of the largest absolute squared set element:

$$\hat{\ell}_\Re = \arg\max_\ell\left\{\left|\tilde{y}_{I,\ell}\right|^2\right\}, \quad \hat{\ell}_\Im = \arg\max_\ell\left\{\left|\tilde{y}_{Q,\ell}\right|^2\right\}. \tag{11}$$

By evaluating every possible combination of *x*, the ML estimator finds an estimation of $\hat{x}$. As a result, the suggested system's ML estimation of the $\hat{x}$ parameter for each of the two *IQ*-components may be written as follows:

$$\hat{x} = \underset{i=1,2,\ldots,M}{\arg\min}\left\{\left|\left(\tilde{y}_{I,\hat{\ell}_\Re} + j\tilde{y}_{Q,\hat{\ell}_\Im}\right) - \sqrt{E_x}\left(\sum_{n=1}^N \alpha_n\beta_n\right) x_i\right|^2\right\}. \tag{12}$$

Eventually, the received bit sequence $\hat{\mathbf{b}}$ is obtained at the receiver side using the bit-back matching approach, the acquired $(\hat{\ell}_\Re, \hat{\ell}_\Im, \hat{x})$ values, and the "Demapper & Sort and Merge" unit.

III. Analysis of the CIM-RIS System's Performance

The average bit error rate analyses of the CIM-RIS system is introduced in this section.

A. Analysis of the CIM-RIS System's Average BER

The entering binary information data is split into two portions, as was already indicated in the system structure of the CIM-RIS approach. As a result, the bit error probability (BEP) of two error events may be used to represent the overall BER expression of the proposed system specified as $\mathcal{P}_{\text{CIM-RIS}}$. In other words, the sum of the BEP of the modulated bits ($\mathcal{P}_{\text{MOD}}$) and the BEP of the mapped bits ($\mathcal{P}_{\text{SC}}$) in the spreading code indices is the total BER that occurs at the receiver. Consequently, the CIM-RIS system's typical average BER statement can be written as follows:

$$\mathcal{P}_{\text{CIM-RIS}} = \frac{2u_2}{u}\mathcal{P}_{\text{SC}} + \frac{u_1}{u}\mathcal{P}_{\text{MOD}}. \tag{13}$$

The average probability of detecting erroneous spreading code indices determines the error events ($\mathcal{P}_{\text{SC}}$) and ($\mathcal{P}_{\text{MOD}}$). Therefore, the correct reception of modulated symbols relies on the correct detection of the spreading code indices at the receiver side of Fig 1. Two main sorts of errors may arise in the CIM-RIS system. The $\hat{\ell}$ are successfully recognized in the first scenario (i.e., the mapped bits of the code indices are right), but the *M*-QAM detector renders the wrong decisions. In the second scenario, the *M*-QAM detector tries to identify bits based on the output of the improperly chosen despreader since the $\hat{\ell}$ are inaccurately detected. In this scenario, the probability of bit error is obviously equal to 0.5 because the receiver has no possibility of selecting the correct choice. The BER equation for modulated bits may thus be written as follows:

$$\mathcal{P}_{\text{MOD}} = \mathcal{P}_M(1-\mathcal{P}_{\text{CI}}) + 0.5\mathcal{P}_{\text{CI}}, \tag{14}$$

where, $\mathcal{P}_M$ stands for BEP for modulated symbols and $\mathcal{P}_{\text{CI}}$ for code indices.

The following two values, $\mathcal{P}_{\text{CI}}$ and u_2, can be used to define the BEP expression of the mapped bits $\mathcal{P}_{\text{SC}}$ of the spreading code indices. The combination of the original spreading code mapping bits will be incorrectly identified if $\hat{\ell}$ is incorrectly estimated. Thus, compared to the original spreading code mapping bits, each incorrect combination will cause the detection of a different amount of incorrect bits. The BER for spreading code indices' bits $\mathcal{P}_{\text{SC}}$ may thus be defined as follows after a few intermediary steps:

$$\mathcal{P}_{\text{SC}} = \frac{\mathcal{P}_{\text{CI}}}{2u_2}. \tag{15}$$

B. The Average Error of Code-Index Detection Probability ($\mathcal{P}_{\text{CI}}$)

The probability that the element with the highest norm value—i.e., this probability—is smaller than the lowest norm value in $|\tilde{y}_{\hat{\ell}}|^2$ for *IQ*-components is known as the probability of the $\mathcal{P}_{\text{CI}}$. As a result, the following definition applies to the probabilities $\mathcal{P}_{\text{CI}}^{\hat{\ell}_{\Re}}$ and $\mathcal{P}_{\text{CI}}^{\hat{\ell}_{\Im}}$ for equiprobable transmitted spreading codes, conditional on the spreading code and channel coefficients:

$$\mathcal{P}_{\text{CI}}^{\hat{\ell}_{\Re}} = \mathcal{P}\left(\left|\tilde{y}_{I,\hat{\ell}_{\Re}}\right|^2 < \min_{\ell\in\{1,2,\ldots,\mathcal{L}\},\ell\neq\hat{\ell}_{\Re}} \left\{\left|\tilde{y}_{\hat{\ell}}\right|^2\right\} \middle| \mathbf{w}_\ell, \mathbf{h}, \mathbf{g}\right) \tag{16}$$

$$\mathcal{P}_{\text{CI}}^{\hat{\ell}_{\Im}} = \mathcal{P}\left(\left|\tilde{y}_{I,\hat{\ell}_{\Im}}\right|^2 < \min_{\ell\in\{1,2,\ldots,\mathcal{L}\},\ell\neq\hat{\ell}_{\Im}} \left\{\left|\tilde{y}_{\hat{\ell}}\right|^2\right\} \middle| \mathbf{w}_\ell, \mathbf{h}, \mathbf{g}\right), \tag{17}$$

where, $\tilde{y}_{I,\hat{\ell}_{\Re}} = \sqrt{E_{x_{\Re}}}\left(\sum_{n=1}^N \alpha_n\beta_n\right)x_{\Re} + \tilde{n}_I$ for $\ell = \hat{\ell}_{\Re}$ and $\tilde{y}_{I,\hat{\ell}_{\Re}} = \tilde{n}_I$ for $\ell \neq \hat{\ell}_{\Re}$; $\tilde{y}_{Q,\hat{\ell}_{\Im}} = \sqrt{E_{x_{\Im}}}\left(\sum_{n=1}^N \alpha_n\beta_n\right)x_{\Im} + \tilde{n}_Q$ for $\ell = \hat{\ell}_{\Im}$ and $\tilde{y}_{Q,\hat{\ell}_{\Im}} = \tilde{n}_Q$ for $\ell \neq \hat{\ell}_{\Im}$. From (16) and (17) it is clear that $\mathcal{P}_{\text{CI}} = \mathcal{P}_{\text{CI}}^{\hat{\ell}_{\Re}} = \mathcal{P}_{\text{CI}}^{\hat{\ell}_{\Im}}$ is used to identify the spreading code indices for the *I* and *Q* channels. As a result, knowing one channel's probability is enough to understand the other. Therefore, it would be appropriate to keep detecting the probability of detecting incorrect *I*-channel spreading code indices. The absolute squared random variables have "non-central chi-square distribution (non-CCSD)" and are independent while $\ell = \hat{\ell}_{\Re}$ and "central chi-square distribution (CCSD)" while $\ell \neq \hat{\ell}_{\Re}$ with even "1"-degrees of freedom since each noise sample at the receiver is multiplied with a distinct spreading code [37].

Then, spreading code index probabilities are derived using the order statistics theory to yield $\mathcal{P}_{\text{CI}}^{\hat{\ell}_{\Re}}$ for the CIM-RIS system. Accordingly, let ξ and λ represent two random variables with the following definitions:

$$\begin{aligned} &\xi = \min\{\xi_\ell\},\ \ \ell \in \{1,2,\ldots,\mathcal{L}\},\ \ \ell \neq \hat{\ell}_{\Re} \\ &\lambda = \left|\tilde{y}_{\hat{\ell}_{\Re}}\right|^2,\ \ \ell = \hat{\ell}_{\Re}, \end{aligned} \tag{18}$$

where $\xi_\ell = |\tilde{y}_\ell|^2$.

In cognizance of (18), ξ_ℓ random variable has a central chi-square distribution (CCSD), but λ follows the non-CCSD. The cumulative distribution function (CDF) of ξ_ℓ follows the CDF of λ with "1" degrees of freedom (DoF) non-CCSD, as do the probability density function (PDF) of ξ_ℓ. These are expressed respectively by [37, (2.3-29, 2.3-24)]:

$$f_\lambda(\lambda) = \frac{1}{2\sigma_\lambda^2}\left(\frac{\lambda}{\kappa_{\hat{\ell}}^2}\right)^{-\frac{1}{4}} e^{-\frac{\kappa_{\hat{\ell}}^2+\lambda}{2\sigma_\lambda^2}} I_{-\frac{1}{2}}\left(\frac{\kappa_{\hat{\ell}}}{\sigma_\lambda^2}\sqrt{\lambda}\right),\ \ \lambda > 0 \tag{19}$$

$$F(\xi_\ell) = 1 - e^{-\frac{\xi_\ell}{2\sigma_{\xi_\ell}^2}} \tag{20}$$

where $I_\beta(y) = \sum_{v=0}^\infty \frac{(y/2)^{\beta+2v}}{v!\Gamma(\beta+v+1)}$, $y \geq 0$ is the modified Bessel function of the first kind and order β [37, (2.3-31)], When the function, $\Gamma(x)$, is represented as $\Gamma(x) = \int_0^\infty t^{x-1}e^{-x}dt$ [37, (2.3-22)]. $\kappa_{\hat{\ell}} = |\sum_{n=1}^N E_c x_{\Re}(\alpha_n e^{-j\theta_n} e^{j\phi_n}\beta_n e^{-j\varphi_n})|$ [37, (2.3-30)], $\sigma_{\xi_\ell}^2 = 2(E_cN_0)^2$ [37, (2.3-25)] and $\sigma_\lambda^2 = 2(E_cN_0)^2 + 4E_cN_0\kappa^2$ [37, (2.3-40)]. Therefore, using order statistics, the probability of $\lambda < \xi$ can be expressed as follows:

$$Pr(\lambda < \xi) = \int_0^\infty Pr(\lambda < \xi) f_\lambda(\lambda)\, d\lambda$$

$$= \int_0^\infty \prod_{\ell=1}^{\mathcal{L}} Pr(\lambda < \xi_\ell) f_\lambda(\lambda) d\lambda. \tag{21}$$

The likelihood of finding incorrect code indices can be stated as follows by using (21):

$$\mathcal{P}_{\mathrm{CI}}^{\hat{\ell}_{\Re}} = \frac{e^{-\frac{\xi_\ell(\mathcal{L}-1)}{2\sigma_{\xi_\ell}^2}}}{2\sigma_\lambda^2} \int_0^\infty \left(\frac{\lambda}{\kappa_{\hat{\ell}}^2}\right)^{-\frac{1}{4}} e^{-\frac{\kappa_{\hat{\ell}}^2+\lambda}{2\sigma_\lambda^2}} I_{-\frac{1}{2}}\left(\frac{\kappa_{\hat{\ell}}}{\sigma_\lambda^2}\sqrt{\lambda}\right) d\lambda. \tag{22}$$

In addition, it becomes clear from (22) that $\mathcal{P}_{\mathrm{CI}}^{\hat{\ell}_{\Re}}$ is still reliant on the random variable (RV) of $\kappa_{\hat{\ell}_{\Re}}$ because of the RV of the Rayleigh fading channel gain. Therefore, $\mathcal{P}_{\mathrm{CI}}^{\hat{\ell}_{\Re}}$ must be integrated over $\kappa_{\hat{\ell}_{\Re}}$'s PDF in order to yield $\mathcal{P}_{\mathrm{CI}}$. Therefore, let $\chi \triangleq \sum_{n=1}^{N} E_c x_{\Re}(\alpha_n e^{-j\theta_n} e^{j\phi_n} \beta_n e^{-j\varphi_n})$ be a RV. The variance of χ is $\sigma_\chi^2 = (x_{\Re}E_c)^2\sigma_h^2$, and its mean is zero. Since $\kappa_{\hat{\ell}_{\Re}} = |\chi|$, the PDF of $\kappa_{\hat{\ell}_{\Re}}$ has a generalized Rayleigh distribution with the PDF of $f(\kappa_{\hat{\ell}_{\Re}}) = \frac{\sqrt{2}}{\sigma_\chi \Gamma(\frac{1}{2})} e^{-\kappa_{\hat{\ell}_{\Re}}^2/2\sigma_\chi^2}$, $\kappa_{\hat{\ell}_{\Re}} \geq 0$ [37, (2.3-52)]. Ultimately, the following can be stated as the average probability of incorrect code-index detection of the CIM-RIS scheme:

$$\mathcal{P}_{\mathrm{CI}} = \int_0^\infty \mathcal{P}_{\mathrm{CI}}^{\hat{\ell}_{\Re}} f\kappa\left(\kappa_{\hat{\ell}_{\Re}}\right) d\kappa_{\hat{\ell}_{\Re}}. \tag{23}$$

Software that does numerical integration may be used to easily determine the integral of the $\mathcal{P}_{\mathrm{CI}}$ equation.

C. Impact of Imperfect Channel State Information on CIM-RIS Technique

In this subsection, it is explored how inaccuracies in channel estimation affect the CIM-RIS system in the absence of perfect CSI at the RIS side and the receiver's end. It is suggested that there is an orthogonal relationship between the estimated channel coefficients and their respective errors, which permits the expressions of $\widehat{h}_{i,j}$ and $\widehat{g}_{i,j}$ in a distinct way, as detailed in [38].

$$\widehat{h}_{i,j} = h_{i,j} + \epsilon_{h_{i,j}},\ \widehat{g}_{i,j} = g_{i,j} + \epsilon_{g_{i,j}}, \tag{24}$$

here, $\widehat{h}$ and $\widehat{g}$ represent the estimated channel coefficients. $\widehat{h}$, $h_{i,j}$, $\widehat{g}$, and $g_{i,j}$ are considered to follow a jointly ergodic and stationary Gaussian process. The expressions $\epsilon_{h_{i,j}}$ and $\epsilon_{g_{i,j}}$ denote the error in channel estimation, modeled as a complex Gaussian variable with zero mean and a variance of σ_ϵ^2, depicted as $\mathcal{CN}(0, \sigma_\epsilon^2)$. In this setting, σ_ϵ^2 indicates the variation in channel estimation accuracy, which can vary depending on the channel estimation methods and the channel's own dynamics. Assuming the use of orthogonal pilot symbols for channel estimation, it has been noted that the estimation error reduces proportionally with an increase in the number of pilot symbols.

D. The Probability of Bit Error of Modulated Bits ($\mathcal{P}_{\mathrm{MOD}}$)

BEP analysis of the error event of the modulated bits ($\mathcal{P}_{\mathrm{MOD}}$) for the CIM-RIS scheme previously given in (14) will be performed in this section. Considering (14), it is seen that $\mathcal{P}_{\mathrm{MOD}}$ depends on two error probabilities, where $\mathcal{P}_{\mathrm{CI}}$ has been previously given in (16) and (17) has been obtained from the (23). Therefore, in order to find $\mathcal{P}_{\mathrm{MOD}}$, $\mathcal{P}_{\mathrm{M}}$ must also be derived.

Considering (6), the mean value and variance of the product of $|\alpha_{\mathrm{n}}|$ and $|\beta_{\mathrm{n}}|$, which are assumed to have separate Rayleigh distributions, are $\mathrm{E}[|\alpha_n||\beta_{\mathrm{n}}|] = 0.25\pi$ and $\mathrm{Var}[|\alpha_n||\beta_{\mathrm{n}}|] = 1 - 0.0625\pi^2$, respectively. The central limit theorem states that $\sum_{n=1}^{N}|\alpha_n||\beta_n|$ converges to a Gaussian distributed RV with statistical parameters $\mathrm{E}[\sum_{n=1}^{N}|\alpha_n||\beta_n|] = 0.25\pi N$ and $\mathrm{Var}[\sum_{n=1}^{N}|\alpha_n||\beta_n|] = (1 - 0.0625\pi^2)N$ for a sufficiently high number of N (i.e., $N >> 1$). Thus, the random variable γ is a non-central chi-square random variable with "1" degree of freedom, and moment-generating function (MGF) $\mathcal{M}_\gamma(s)$ of the γ can be given as follows [39]:

$$\mathcal{M}_\gamma(s) \approx \left(\frac{\mathcal{U}_1}{\mathcal{U}_1 + s\bar{\gamma}}\right)^{\frac{1}{2}} \exp\left(-\frac{s\,\bar{\gamma}\,\mathcal{U}_2}{\mathcal{U}_2 + s\bar{\gamma}}\right), \tag{25}$$

where $\mathcal{U}_1 = \frac{8}{N(16-\pi^2)}, \mathcal{U}_2 = \frac{N\pi^2}{2(16-\pi^2)}$, and $\bar{\gamma} = \frac{E_x}{N_0}$.

Since the proposed system model works well at low SNR region, approximation of the MGF expression in (25) can be expressed as follows:

$$\mathcal{M}_\gamma(s) \approx \exp\left(-\frac{\mathcal{U}_2}{\mathcal{U}_1} s\bar{\gamma}\right). \tag{26}$$

On the other hand, the ASER expression of QAM at low SNR region can be given as follows [39]:

$$\begin{aligned}\mathcal{P}_{\mathrm{QAM}} &= 2p\mathcal{F}(t, \pi/2) + 2q\mathcal{F}(z, \pi/2) - 2pq \\ &\quad \times[\mathcal{F}(z, \arctan(z/t)) + \mathcal{F}(t, \mathrm{arccot}(z/t))],\end{aligned} \tag{27}$$

where, $p = 1 - \frac{1}{M_I}$ and $q = 1 - \frac{1}{M_Q}$, here M_I is the number of in-phase points in the constellation, while M_Q is the number of quadrature points in the constellation. t is expressed as $t = \sqrt{\frac{6}{(M_I^2-1)+(M_Q^2-1)\beta^2}}$, and z is expressed as $z = \beta t$. In this study, $M_I = M_Q = \sqrt{M}$ and $\beta = 1$ are used as special cases, since the number of in-phase and quadrature elements of QAM constellations are equal. Also, the integral $\mathcal{F}(\cdot,\cdot)$ is given as follows:

$$\mathcal{F}(x, \theta) = \frac{1}{\pi}\int_0^\theta \mathcal{M}_\gamma\left(\frac{x^2}{2\sin^2\phi}\right) d\phi. \tag{28}$$

Eq. (28) can be upper bound to obtain insights by setting $\phi = \theta$, which results in:

$$\begin{aligned}\mathcal{F}(x, \theta) &\leq \frac{\theta}{\pi}\mathcal{M}_\gamma\left(\frac{x^2}{2\sin^2\theta}\right) \\ &\leq \frac{\theta}{\pi}\exp\left(-\frac{\mathcal{U}_2 x^2\bar{\gamma}}{2\mathcal{U}_1\sin^2\theta}\right) \\ &\leq \frac{\theta}{\pi}\exp\left(-\frac{N^2\pi^2x^2\bar{\gamma}}{32\sin^2\theta}\right).\end{aligned} \tag{29}$$

As a result, $\mathcal{P}_{\mathrm{M}}$ with the QAM constellation scheme can be expressed as follows:

$$\begin{aligned}\mathcal{P}_{\mathrm{M}} = \frac{1}{u_1}\Bigg[&p\exp\left(-12\left(\frac{\pi^2t^2}{32}\right)N^2\bar{\gamma}\right) + q\exp\left(-\left(\frac{\pi^2z^2}{32}\right)N^2\bar{\gamma}\right) \\ &-\frac{2pq}{\pi}\left[\arctan\left(\frac{z}{t}\right)\exp\left(-\left(\frac{\pi^2(t^2+z^2)}{32}\right)N^2\bar{\gamma}\right)\right.\end{aligned}$$

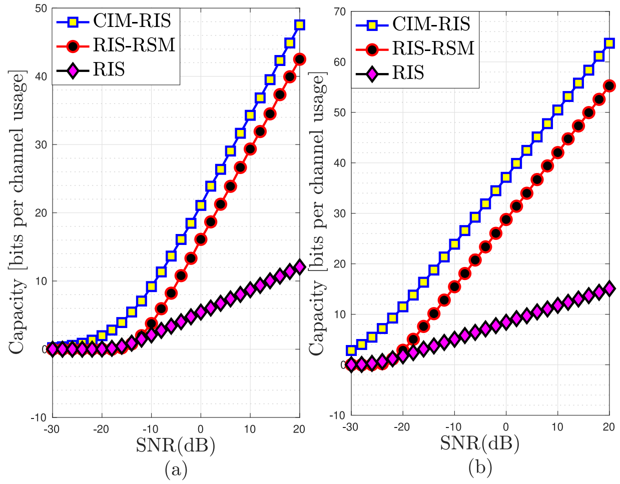

Fig. 2. Capacity comparisons of the CIM-RIS, RIS-RSM and RIS systems while $N = 16$ for (a) and $N = 64$ for (b).

$$+ \operatorname{arccot}\left(\frac{z}{t}\right) \exp\left(-\left(\frac{\pi^2(t^2+z^2)}{32}\right) N^2 \bar{\gamma}\right)\Bigg]\Bigg], \tag{30}$$

Finally, when $\mathcal{P}_{\mathrm{M}}$ and $\mathcal{P}_{\mathrm{CI}}$ are substituted to (14), $\mathcal{P}_{\mathrm{MOD}}$ is obtained. The analytical average total probability of the error for the CIM-RIS system is therefore calculated by putting (14), and (15) into (13).

IV. Capacity Analyses

The derivations of capacity analysis for the proposed CIM-RIS system are presented in this section. The capacity of the proposed CIM-RIS system can be expressed separately for I and Q components. However, since the capacity for I and Q components are the same, only the capacity for I component is analyzed in this section.

The ergodic capacity expression of a conventional MIMO system can be given as follows [40]:

$$\mathcal{C} = \mathrm{E}_{\mathbf{h}}\left\{\max_{P_{x_i}} I(x_i; \mathbf{y} \mid \mathbf{h})\right\}. \tag{31}$$

$I(c_i; \mathbf{y} \mid \mathbf{h})$ represents the mutual information between the transmitted vector x_i and the received vector $\mathbf{y} = [y_1, y_2, \ldots, y_{N_R}]^T \in \mathbb{C}^{n_R \times 1}$ given a known $\mathbf{h}$. Where N_R is the number of receive antennas of the MIMO system. In the proposed CIM-RIS system, unlike the conventional MIMO system, data is transmitted not only in conventional symbols but also in spreading code indices. Thus, the capacity of the proposed CIM-RIS system is determined by maximizing the mutual information between the M-QAM symbol and the active spreading code indices in $\mathbf{y}$. Consequently, based on [41], the capacity of the proposed CIM-RIS system is expressed as follows:

$$\mathcal{C} = \mathrm{E}_{\mathcal{H}}\left\{\max_{\mathcal{P}_{\mathbf{f}_\ell}, \mathcal{P}_{\mathbf{x}_{\Re}}} I(\mathbf{f}_\ell, x_{\Re}; \mathbf{y})\right\}, \tag{32}$$

where $\mathcal{H} = \mathbf{h}^T \mathbf{\Phi} \mathbf{g}$ and $\mathbf{f}_\ell \in \mathbb{C}^{\mathcal{L} \times 1} \triangleq [0\ 0 \cdots 0, \underset{\ell^{\text{th}}\ \text{index}}{\underset{\uparrow}{1}}, 0\ \ldots, 0\ 0]^T$ is the vector that indicates the position of the active spreading code index $\ell_{\Re}^{\text{th}}$ for the I component. In this vector, the element corresponding to the active spreading code index is represented as 1, while the other elements are represented as 0. The received signal, expressed in vector-matrix form, can be redefined as follows:

$$\mathbf{y} = \sqrt{E_{x_{\Re}}}\, \mathcal{H}\, \mathbf{W}\, \mathbf{f}_\ell\, x_{\Re} + \mathbf{n}, \tag{33}$$

where $\mathbf{W} \in \mathbb{C}^{K \times \mathcal{L}} = [\mathbf{w}_1, \mathbf{w}_2, \ldots, \mathbf{w}_{\mathcal{L}}]$ is the code matrix containing all spreading codes. The mutual information $I(\mathbf{f}_\ell, x_{\Re}; \mathbf{y})$, indicating the number of data bits accurately received by the receiver in the proposed CIM-RIS system as described in (32), is expressed as follows:

$$I(\mathbf{f}_\ell, x_{\Re}; \mathbf{y}) = \mathrm{H}(\mathbf{y}) - \mathrm{H}\big(\mathbf{y} \mid \mathbf{f}_\ell, x_{\Re}\big), \tag{34}$$

where $\mathrm{H}(.)$ denotes the entropy function. When $\mathbf{f}_\ell$ and $x_{\Re}$ are known, the entropy of $\mathbf{y}$ is expressed as follows:

$$\mathrm{H}\big(\mathbf{y} \mid \mathbf{f}_\ell, x_{\Re}\big) = \mathrm{H}(\mathbf{n}) = \log_2 \left|\pi e N_0 \mathbf{I}_K\right|. \tag{35}$$

Here, $\mathbf{I}_K$ is the identity matrix with K dimensions. $e \sim \mathcal{CN}(0, N_0\mathbf{I}_K)$ and $\mathbf{y} \sim \mathcal{CN}(\mu_{\mathbf{y}}, \sigma_{\mathbf{y}}^2 \mathbf{I}_K)$ follow complex Gaussian distributions with $\mu_{\mathbf{y}} = \frac{N\sqrt{\pi}}{2}$ and $\sigma_{\mathbf{y}}^2 = \frac{N(4-\pi)}{4}$. Furthermore, in (35), the expression mutual information $I(\mathbf{f}_\ell, x_{\Re}; \mathbf{y})$ for the proposed CIM-RIS system is maximized only when $\mathrm{H}(\mathbf{y})$ is maximized. Thus, $\mathrm{H}(\mathbf{y})$ is given as follows:

$$\mathrm{H}(\mathbf{y}) = -\,\mathrm{E}_{\mathbf{y}}\{\log_2 \mathcal{P}(\mathbf{y})\} = \log_2 \left|\pi e \mathcal{R}_{\mathbf{yy}}\right|, \tag{36}$$

where $\mathcal{R}_{\mathbf{yy}}$ represents the covariance matrix of the $\mathcal{H}\mathbf{W}\mathbf{f}_\ell x_{\Re}$ defined as follows:

$$\begin{aligned}\mathcal{R}_{\mathbf{yy}} &= E\left(\mathbf{y}\mathbf{y}^H \middle| \mathbf{f}_\ell\right) \\ &= \frac{1}{\mathcal{L}} \sum_{\ell=1}^{\mathcal{L}} \mathcal{H}\mathbf{W}\mathbf{f}_\ell \mathbf{f}_\ell^H \mathbf{W}^H \mathcal{H}^* + N_0 \mathbf{I}_K.\end{aligned} \tag{37}$$

As a result, with the help of the expressions obtained above, the capacity of the proposed CIM-RIS system is obtained as follows:

$$\mathcal{C} = \mathrm{E}_{\mathcal{H}}\left\{\log_2 \det\left(\mathbf{I}_K + \frac{\sum_{\ell=1}^{n_S} \mathcal{H}\mathbf{W}\mathbf{f}_\ell \mathbf{f}_\ell^H \mathbf{W}^H \mathcal{H}^*}{\mathcal{L} N_0}\right)\right\}. \tag{38}$$

Fig. 2 displays the capacity comparisons of CIM-RIS, RIS-RSM, and RIS systems with $N = 16$ for (a) and $N = 64$ for (b). The capacity comparisons in Fig. 2 are based on system parameters $\mathcal{L} = K = 4$ for CIM-RIS scheme and $N_R = 4$ for RIS-RSM scheme. From Fig. 2, it is readily observed that the capacities of all systems are augmented as the number of reflecting surfaces N increases. Furthermore, it is noted that the proposed CIM-RIS system exhibits a superior capacity compared to the RIS-RSM and RIS systems.

V. The Analysis of Energy Efficiency, Throughput, and Data Rate

In this section, energy efficiency, throughput, and data rate analyses of CIM-RIS, TSM-RIS, TQSM-RIS, and traditional RIS systems are performed.

TABLE I
COMPARISONS OF THE CIM-RIS SYSTEM'S ENERGY SAVINGS IN RELATION TO OTHER SYSTEMS, EXPRESSED AS A PERCENTAGE (E_{sav} %)

M	N_T	$\mathcal{L}$	RIS	TSM-RIS	TQSM-RIS
4	2	4	66.7	50	33.4
8	8	16	72.2	45.6	18.9
32	16	32	66.7	44.4	13.3

TABLE II
A COMPARATIVE EVALUATION OF THE COMPUTATIONAL COMPLEXITY

Systems	Reel Multiplications (RMs)
$\mathcal{O}_{\text{CIM-RIS}}$	$8K\mathcal{L}+N+4M$
$\mathcal{O}_{\text{RIS}}$	$(N+4M)\left(1+\frac{2u_2}{\log_2(M)}\right)$
$\mathcal{O}_{\text{TSM-RIS}}$	$8(N+4M)N_T\left(1+\frac{2u_2}{\eta_{SM}}\right)$
$\mathcal{O}_{\text{TQSM-RIS}}$	$8(N+4M)N_T\left(1+\frac{2u_2}{\eta_{QSM}}\right)$

A. The Energy Efficiency Analysis

In this section, the energy-saving percentages of the CIM-RIS system are given compared to the TSM-RIS, TQSM-RIS and traditional RIS systems. In the proposed CIM-RIS system, very little energy consumption occurs as most of the data bits are transmitted in spreading code indices. Therefore, the proposed CIM-RIS system is a high energy efficient system. As a result, the energy-saving percentage ($\mathcal{E}_{\text{sav}}$) per u bits of the CIM-RIS system compared to the benchmark systems can be given as follows:

$$\mathcal{E}_{\text{sav}} = \left(1 - \frac{u_b}{u}\right) E_b\%. \tag{39}$$

where u_b is the spectral efficiencies of the benchmark systems and E_b represents the bit energy. In Table I, the percentage of energy saving provided by the CIM-RIS system compared to the benchmark systems is given depending on the changing M, transmit antenna number (N_T), and $\mathcal{L}$ values.

Explaining this with an example can aid readers in better following the publication. Explaining the first row of Table I will be beneficial for understanding better. The CIM-RIS system transmits $\log_2(M) = \log_2(4) = 2$ bits through symbol and sends an additional $2 \times \log_2(\mathcal{L}) = 2\log_2(4) = 4$ bits through code indices, totaling 6 bits. In contrast, a conventional RIS system transmits only $\log_2(M) = \log_2(4) = 2$ bits solely via the symbol. Consequently, the CIM-RIS system transmits an extra $(6-2) = 4$ bits during the same channel use, resulting in an energy efficiency of 4/6, which equates to approximately 66.7%. Similarly, the TSM-RIS system transmits $\log_2(N_T) = \log_2(2) = 1$ bit via the antenna and $\log_2(M) = \log_2(4) = 2$ bits via the symbol, totaling 3 bits. Hence, the CIM-RIS system transmits an additional $(6-3) = 3$ bits in the same channel use, achieving an energy efficiency of 3/6, or 50%. Lastly, the TQSM-RIS system sends $2 \times \log_2(N_T) = 2 \times \log_2(2) = 2$ bits via the antenna and $\log_2(M) = \log_2(4) = 2$ bits via the symbol, totaling 4 bits. Thus, the CIM-RIS system transmits an extra $(6-4) = 2$ bits during the same channel use, leading to an energy efficiency of 2/6, or approximately 33.4%.

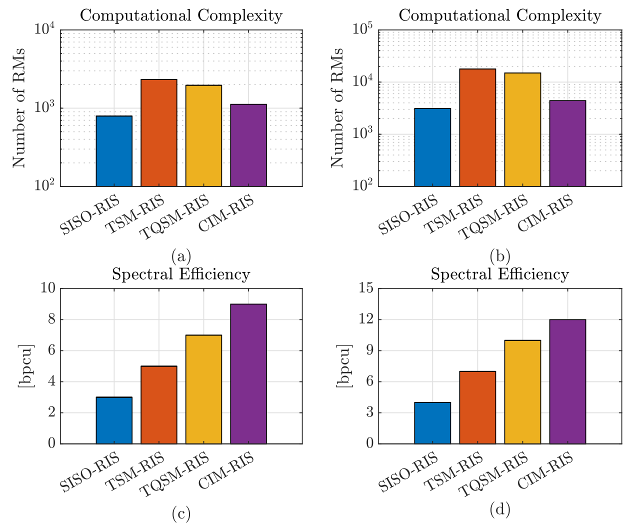

Fig. 3. Computational Complexity and Spectral Efficiency Comparisons while $M = 8$, $N_T = 4$, $\mathcal{L} = 8$, $K = 16$ $N = 64$ for (a), (c); and $M = 16$, $N_T = 8$, $\mathcal{L} = 16$, $K = 32$ $N = 256$ for (b), (d).

B. System Complexity Analysis

In this section, computational complexity analyses of traditional RIS, TSM-RIS, TQSM-RIS, and CIM-RIS systems in terms of real multiplications (RMs) are obtained. The computational complexity results of the proposed CIM-RIS system according to the benchmark systems are given in Table II. Computational complexity and spectral efficiency comparisons of the RIS, TSM-RIS, TQSM-RIS, and CIM-RIS systems are given in Fig. 3. Where, 3, $M = 8$, $N_T = 4$, $\mathcal{L} = 8$, $K = 16$ $N = 64$ parameters are used for (a), (c); and $M = 16$, $N_T = 8$, $\mathcal{L} = 16$, $K = 32$ $N = 256$ parameters are selected for (b), (d). As can be seen from Fig. 3, the CIM-RIS system gives better results than the benchmark systems, both in terms of spectral efficiency and computational complexity. Consequently, according to all the results obtained, it is understood that the CIM-RIS system is a high data rate and low complexity technique.

C. The CIM-RIS System's Throughput and Data Rate Analysis

The amount of accurate bits that a unit has acquired in a certain amount of time is typically used to indicate the throughput of a communication system. So, the CIM-RIS scheme's throughput can be expressed as follows [42]:

$$\mathcal{T} = \frac{(1 - \mathcal{P}_{\text{GCIM-SM}})}{\tau_s} u, \tag{40}$$

where $(1 - \mathcal{P}_{\text{GCIM-SM}})$ is the probability that the right bits were received for the entire symbol's duration τ_s.

The throughput comparisons can be carried out fairly since the τ_s symbol durations for traditional RIS, TSM-RIS, and TQSM-RIS approaches are the identical. Table III presents data rate comparisons for different N_T, M, and $\mathcal{L}$ values.

With instance, the CIM-RIS system sends 9 bits for the same symbol time τ_s for $N_T = 4$, $M = 8$, and $\mathcal{L} = 8$, while the TSM-RIS, TQSM-RIS, and traditional RIS schemes transmit 5 bits, 7 bits, and 3 bits respectively.

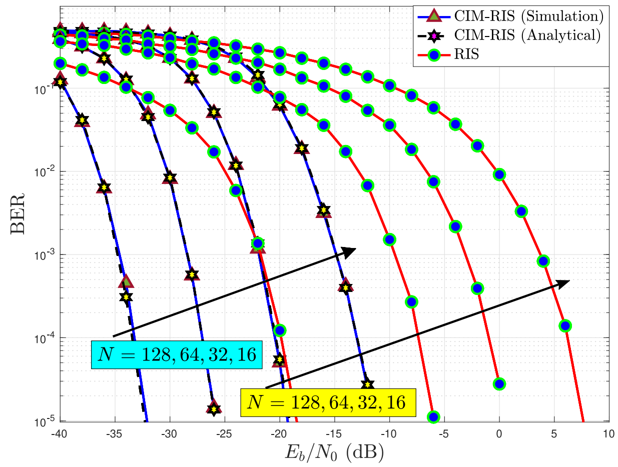

Fig. 4. BER performance comparisons of CIM-RIS and RIS systems for $u = 10$ bits when N=16, 32, 64, and 128.

TABLE III
COMPARISONS OF DATA RATES (BITS PER τ_s)

N_T	M	$\mathcal{L}$	CIM-RIS	TSM-RIS	TQSM-RIS	RIS
2	4	8	8	3	4	2
4	8	8	9	5	7	3
8	8	16	11	6	9	3

VI. SIMULATION RESULTS

Results from computer simulations using the CIM-RIS, Transmit SM-RIS (TSM-RIS), Transmit QSM-RIS (TQSM-RIS), and traditional RIS approaches are provided and compared in this section in the presence of Rayleigh fading channels. The received symbols and indices are estimated at the receiver using the ML method. Using the Monte Carlo simulation approach, average BER performances were obtained. u is the number of bits a symbol is carrying. The SNR applied in the simulations is denoted by the $\mathrm{SNR(dB)} = 10\log_{10}(E_b/N_0)$, where $E_b = E_s/u$, here $E_s = \sum_{k=1}^{K}(w_{i,k}/\sqrt{K})^2$ denotes the average symbol energy. The spreading code length "K" for performance comparisons is chosen as 32.

In Fig. 4, the analytical and simulation BER performance curves of the CIM-RIS and traditional RIS systems are presented for N=16, 32, 64, and 128 in case of $u = 10$ bits. In Fig. 4, the CIM-RIS system with $M = 4$ and $\mathcal{L} = 16$ transmits $2u_2 = 8$ bits of $u = 10$ bits in the spreading code index and $u_1 = 2$ bits via the 4-QAM symbol. On the other hand, traditional RIS system transmits all $u = 10$ bits in the 1024-QAM symbol. The proposed CIM-RIS system provides SNR gains of 13.5 dB,19.57 dB,19.86 dB, and 18.85 dB compared to the conventional RIS system when the number of reflective surfaces is selected as N=16, 32, 64, 128 respectively. According to the computer simulations carried out, it is seen that the performance of the system increases significantly in direct proportion to the number of RIS elements in the CIM-RIS system.

Fig. 5 compares the BER performance of the CIM-RIS system, the TSM-RIS system, the TQSM-RIS system, and the conventional RIS system for $N = 128$ and $u = 8$ bits.

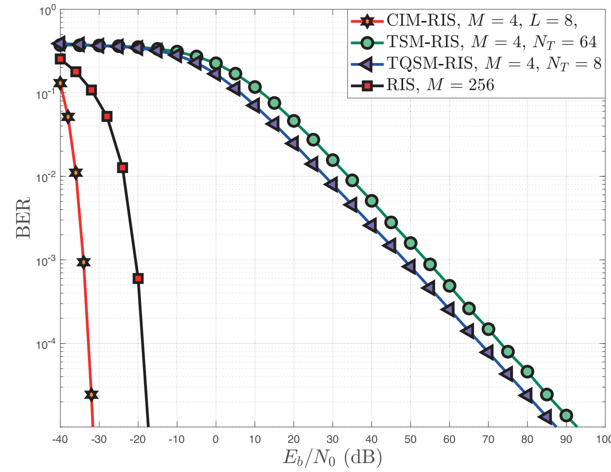

Fig. 5. BER performance comparisons of CIM-RIS, TSM-RIS, TQSM-RIS, and traditional RIS systems for $u = 8$ bits when $N = 128$.

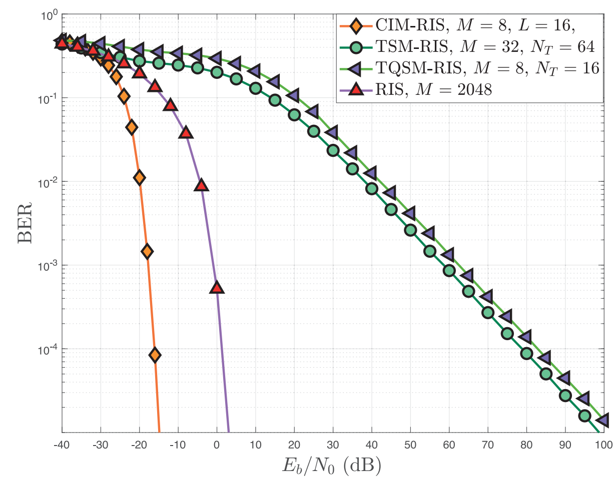

Fig. 6. BER performance comparisons of CIM-RIS, TSM-RIS, TQSM-RIS, and traditional RIS systems for $u = 11$ bits when $N = 32$.

Comparing the proposed CIM-RIS system to the conventional RIS system, an SNR gain of around 14.2 dB is achieved. In addition, the CIM-RIS system offers an SNR gain of around 119 dB compared to the TQSM-RIS system and about 124 dB compared to the TSM-RIS system.

In Fig. 6, the BER performance comparisons of the CIM-RIS system, TSM-RIS system, TQSM-RIS, and traditional RIS system are presented for $N = 32$, in the case of $u = 11$ bits. The proposed CIM-RIS system provides an SNR gain of about 112.8 dB compared to the TSM-RIS system, while it provides an SNR gain of about 117.68 dB compared to the TQSM-RIS system. Besides, the CIM-RIS system provides an SNR gain of about 18 dB compared to the traditional RIS system. If Fig. 6 is considered carefully, it can be seen that the TSM-RIS system is more performant than the TQSM-RIS system. The fact that the TSM-RIS system provides a BER performance improvement of about 5 dB compared to the TQSM-RIS system can be explained by the fact that the TSM-RIS system transmits 5 bits of 11 bits over RIS and the other 6 bits over antenna indices. On the other hand, the TQSM-RIS system transmits only 3 bits directly over RIS and 8 bits directly over antenna indices. In TSM-RIS or TQSM-RIS schemes,

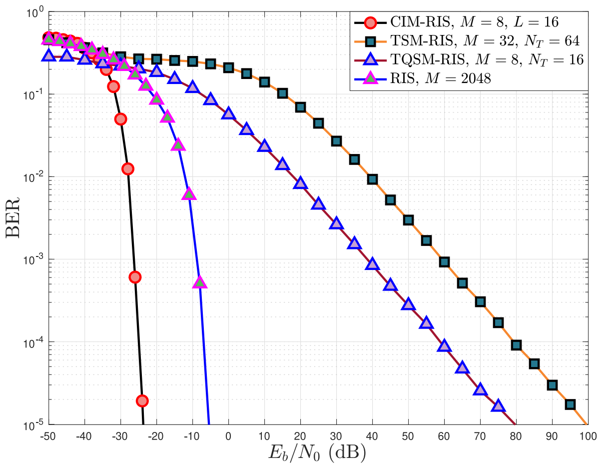

Fig. 7. BER performance comparisons of CIM-RIS, TSM-RIS, TQSM-RIS, and traditional RIS systems for $u = 11$ bits, $N = 64$ over Rician fading channels.

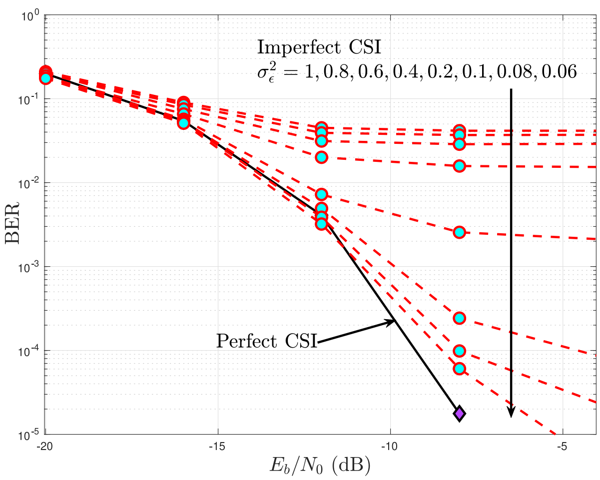

Fig. 8. BER performance of CIM-RIS system under the impact of imperfect channel knowledge for $u = 11$ bits when $N = 16$.

transmitting data directly over the antenna indices instead of transmitting data over RIS deteriorates the performance.

In Fig. 7, the BER performance comparisons of the CIM-RIS system, TSM-RIS system, TQSM-RIS, and traditional RIS system are presented for $N = 64$, in the case of $u = 11$ bits over Rician fading channels. Here the Rician $\mathcal{K}$ parameter is chosen as $\mathcal{K} = 5$ and all simulations are performed accordingly. The proposed CIM-RIS system provides an SNR gain of about 123.72 dB compared to the TSM-RIS system, while it provides an SNR gain of about 103.67 dB compared to the TQSM-RIS system. Besides, the CIM-RIS system provides an SNR gain of about 18.36 dB compared to the traditional RIS system.

Fig. 8 presents an analysis of the BER performance of the CIM-RIS system under Rayleigh fading channels in terms of perfect and imperfect CSI. This analysis is based on simulations conducted with parameters $u = 11$ bits and $N = 16$ while $M = 8$ and $\mathcal{L} = 16$. During the examination of system performance, the ${\sigma_\epsilon}^2$ values were sequentially set to 1, 0.8, 0.6, 0.4, 0.2, 0.1, 0.08, and 0.06 to observe their impact on imperfect CSI in CIM-RIS. The results obtained indicate a noticeable improvement in BER as the ${\sigma_\epsilon}^2$ value decreases.

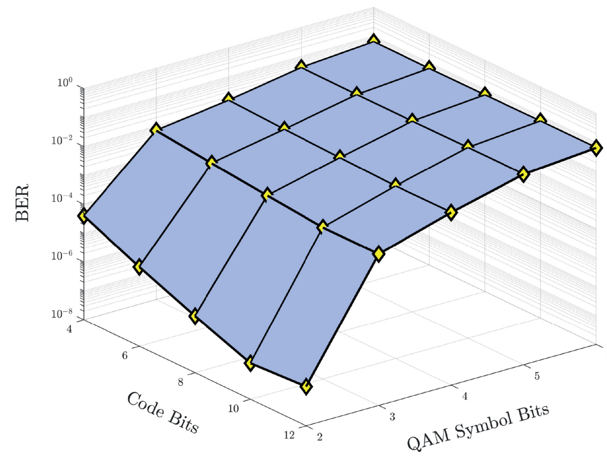

Fig. 9. 3D BER performance of the CIM-RIS system for $K = 128$, $N = 64$, and SNR $= -25$ dB.

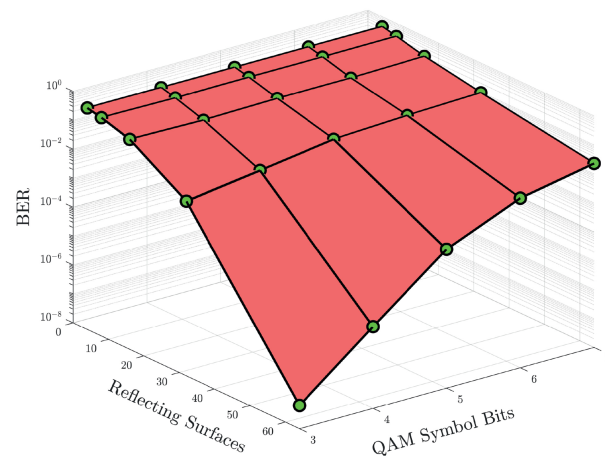

Fig. 10. 3D BER performance of the CIM-RIS system for $K = 32$, $\mathcal{L} = 16$, and SNR $= -20$ dB.

Fig. 9 presents the 3D error performance results depending on the bits carried in the symbol and the spreading code index. Where the selected parameter values are M=4,8,16,32,64 and $\mathcal{L} = 4, 8, 16, 32, 64$. As can be seen from Fig. 9, the error performance worsens as the number of bits carried from the symbol increases, while the error performance improves as the number of bits carried in the spreading code index increases.

The 3D error performance of the CIM-RIS system, which varies according to the number of bits carried in the spreading code index and the number of reflecting surfaces, is given the Fig. 10. In this simulation, M=8,16,32,64 and N=4,8,16,32 values are used. The obtained results show that the increase in the number of reflective surfaces reduces the error.

As a result, when all the aforementioned Figures are considered, it can be easily said that the proposed CIM-RIS system causes a significant increase in performance compared to the TSM-RIS, TQSM-RIS, and the traditional RIS techniques.

VII. Conclusion

In this study, a novel MIMO transmission system with high data-rate, high energy efficiency, and good error performance is proposed for Rayleigh fading channels by combining RIS and CIM techniques, which are potential and promising techniques for next-generation wireless communication networks. It has been shown via computer simulations that the CIM-RIS system has better error performance, lower transmission energy, faster data transmission rate, and compared to the TSM-RIS, TQSM-RIS, and the traditional RIS systems. In addition, the energy efficiency, complexity analysis, throughput, and bit error rate of the proposed technique are derived. The capacity analysis of the proposed CIM-RIS system is obtained by utilizing mutual information. It is also shown that the proposed system has a higher capacity compared to counterpart wireless communication systems in the literature for different system parameters. The simulation results demonstrate that the proposed CIM-RIS technique has more performance than traditional RIS, TSM-RIS, and TQSM-RIS communication techniques. In addition, due to the nature of CIM, which is the building block of the CIM-RIS technique, it uses less energy than the systems discussed above. The investigation has been extended to cover the CIM-RIS system's performance under Rician fading channels. In addition, the performance of the proposed system under conditions of imperfect channel state information (CSI) has also been obtained and illustrated.

REFERENCES

[1] F. Cogen and E. Aydin, "Hexagonal quadrature amplitude modulation aided spatial modulation," in *Proc. 11th Int. Conf. Elect. Electron. Eng. (ELECO)*, 2019, pp. 730–733.

[2] S. K. Sharma, I. Woungang, A. Anpalagan, and S. Chatzinotas, "Towards tactile Internet in beyond 5G era: Recent advances, current issues and future directions," *IEEE Access*, vol. 8, pp. 56948–56991, 2020.

[3] E. Aydin, F. Cogen, and E. Basar, "Code-index modulation aided quadrature spatial modulation for high-rate MIMO systems," *IEEE Trans. Veh. Technol.*, vol. 68, no. 10, pp. 10257–10261, Oct. 2019.

[4] F. Cogen, E. Aydin, N. Kabaoglu, E. Basar, and H. Ilhan, "Generalized code index modulation and spatial modulation for high rate and energy-efficient MIMO systems on rayleigh block-fading channel," *IEEE Syst. J.*, vol. 15, no. 1, pp. 538–545, Mar. 2020.

[5] F. Cogen, E. Aydin, N. Kabaoglu, E. Basar, and H. Ilhan, "A novel MIMO scheme based on code-index modulation and spatial modulation," in *Proc. 26th Signal Process. Commun. Appl. Conf. (SIU)*, 2018, pp. 1–4.

[6] X. Cheng, M. Zhang, M. Wen, and L. Yang, "Index modulation for 5G: Striving to do more with less," *IEEE Wireless Commun. Mag.*, vol. 25, no. 2, pp. 126–132, Apr. 2018.

[7] M. Wen, X. Cheng, and L. Yang, *Index Modulation for 5G Wireless Communications*. Cham, Switzerland: Springer, 2017.

[8] B. A. Ozden, F. Cogen, and E. Aydin, "Mirror activation pattern selection for energy efficient hexagonal QAM aided media-based modulation," *Trans. Emerg. Telecommun. Technol.*, vol. 34, no. 7, 2023, Art. no. e4795.

[9] G. Kaddoum, Y. Nijsure, and H. Tran, "Generalized code index modulation technique for high-data-rate communication systems," *IEEE Trans. Veh. Technol.*, vol. 65, no. 9, pp. 7000–7009, Nov. 2016.

[10] E. Aydin, "EDAS/COAS based antenna selection for code index modulation aided spatial modulation," *Electrica*, vol. 19, no. 2, pp. 113–119, Jul. 2019.

[11] B. A. Ozden, E. Aydin, and F. Cogen, "Code index modulation-aided spatial media-based modulation system for future wireless networks," *IEEE Syst. J.*, vol. 17, no. 3, pp. 3762–3770, Sep. 2023.

[12] R. Y. Mesleh, H. Haas, S. Sinanovic, C. W. Ahn, and S. Yun, "Spatial modulation," *IEEE Trans. Veh. Technol.*, vol. 57, no. 4, pp. 2228–2241, Jul. 2008.

[13] C. Huang et al., "Reconfigurable intelligent surfaces for energy efficiency in wireless communication," *IEEE Trans. Wireless Commun.*, vol. 18, no. 8, pp. 4157–4170, Aug. 2019.

[14] W. Tang et al., "MIMO transmission through reconfigurable intelligent surface: System design, analysis, and implementation," *IEEE J. Sel. Areas Commun.*, vol. 38, no. 11, pp. 2683–2699, Nov. 2020.

[15] M. Di Renzo et al., "Reconfigurable intelligent surfaces vs. relaying: Differences, similarities, and performance comparison," *IEEE Open J. Commun. Soc.*, vol. 1, pp. 798–807, 2020.

[16] E. Basar, "Reconfigurable intelligent surface-based index modulation: A new beyond MIMO paradigm for 6G," *IEEE Trans. Commun.*, vol. 68, no. 5, pp. 3187–3196, May 2020.

[17] L. Subrt and P. Pechac, "Controlling propagation environments using intelligent walls," in *Proc. Eur. Conf. Antennas Propag. (EUCAP)*, 2012, pp. 1–5.

[18] X. Tan, Z. Sun, J. M. Jornet, and D. Pados, "Increasing indoor spectrum sharing capacity using smart reflect-array," in *Proc. IEEE Int. Conf. Commun. (ICC)*, 2016, pp. 1–6.

[19] C. Huang, A. Zappone, M. Debbah, and C. Yuen, "Achievable rate maximization by passive intelligent mirrors," in *Proc. IEEE ICASSP*, 2018, pp. 3714–3718.

[20] C. Huang, G. C. Alexandropoulos, A. Zappone, M. Debbah, and C. Yuen, "Energy efficient multi-user MISO communication using low resolution large intelligent surfaces," in *Proc. IEEE Globecom Workshops (GC Wkshps)*, 2018, pp. 1–6.

[21] Q. Wu and R. Zhang, "Intelligent reflecting surface enhanced wireless network via joint active and passive beamforming," *IEEE Trans. Wireless Commun.*, vol. 18, no. 11, pp. 5394–5409, Nov. 2019.

[22] Q. Wu and R. Zhang, "Beamforming optimization for wireless network aided by intelligent reflecting surface with discrete phase shifts," *IEEE Trans. Commun.*, vol. 68, no. 3, pp. 1838–1851, Mar. 2020.

[23] X. Yu, D. Xu, and R. Schober, "MISO wireless communication systems via intelligent reflecting surfaces," in *Proc. IEEE/CIC Int. Conf. Commun. China (ICCC)*, 2019, pp. 735–740.

[24] E. Basar, "Transmission through large intelligent surfaces: A new frontier in wireless communications," in *Proc. Eur. Conf. Netw. Commun. (EuCNC)*, 2019, pp. 112–117.

[25] A. Khaleel and E. Basar, "Reconfigurable intelligent surface-empowered MIMO systems," *IEEE Syst. J.*, vol. 15, no. 3, pp. 4358–4366, Sep. 2021.

[26] Z. Yigit, E. Basar, and I. Altunbas, "Low complexity adaptation for reconfigurable intelligent surface-based MIMO systems," *IEEE Commun. Lett.*, vol. 24, no. 12, pp. 2946–2950, Dec. 2020.

[27] A. E. Canbilen, E. Basar, and S. S. Ikki, "Reconfigurable intelligent surface-assisted space shift keying," *IEEE Wireless Commun. Lett.*, vol. 9, no. 9, pp. 1495–1499, May 2020.

[28] Q. Wu and R. Zhang, "Towards smart and reconfigurable environment: Intelligent reflecting surface aided wireless network," *IEEE Commun. Mag.*, vol. 58, no. 1, pp. 106–112, Jan. 2020.

[29] E. Basar, M. Di Renzo, J. De Rosny, M. Debbah, M.-S. Alouini, and R. Zhang, "Wireless communications through reconfigurable intelligent surfaces," *IEEE Access*, vol. 7, pp. 116753–116773, 2019.

[30] M. Di Renzo et al., "Smart radio environments empowered by reconfigurable AI meta-surfaces: An idea whose time has come," *EURASIP J. Wireless Commun. Netw.*, vol. 2019, no. 1, pp. 1–20, May 2019.

[31] B. A. Ozden, E. Aydin, and F. Cogen, "Reconfigurable intelligent surface-aided spatial media-based modulation," *IEEE Trans. Green Commun. Netw.*, vol. 7, no. 4, pp. 1971–1980, Dec. 2023.

[32] Q. Li, M. Wen, and M. Di Renzo, "Single-RF MIMO: From spatial modulation to metasurface-based modulation," *IEEE Wireless Commun.*, vol. 28, no. 4, pp. 88–95, Aug. 2021.

[33] S. Guo, S. Lv, H. Zhang, J. Ye, and P. Zhang, "Reflecting modulation," *IEEE J. Sel. Areas Commun.*, vol. 38, no. 11, pp. 2548–2561, Nov. 2020.

[34] W. Yan, X. Yuan, Z.-Q. He, and X. Kuai, "Passive beamforming and information transfer design for reconfigurable intelligent surfaces aided multiuser MIMO systems," *IEEE J. Sel. Areas Commun.*, vol. 38, no. 8, pp. 1793–1808, Aug. 2020.

[35] S. Lin, B. Zheng, G. C. Alexandropoulos, M. Wen, M. D. Renzo, and F. Chen, "Reconfigurable intelligent surfaces with reflection pattern modulation: Beamforming design and performance analysis," *IEEE Trans. Wireless Commun.*, vol. 20, no. 2, pp. 741–754, Feb. 2021.

[36] Q. Li, M. Wen, E. Basar, G. C. Alexandropoulos, K. J. Kim, and H. V. Poor, "Channel estimation and multipath diversity reception for RIS-empowered broadband wireless systems based on cyclic-prefixed single-carrier transmission," *IEEE Trans. Wireless Commun.*, vol. 22, no. 8, pp. 5145–5156, Aug. 2023.

[37] J. G. Proakis and M. Salehi, *Digital Communications 5th Edition*. New York, NY, USA: McGraw-Hill, 2007.

[38] R. Mesleh and S. S. Ikki, "On the impact of imperfect channel knowledge on the performance of quadrature spatial modulation," in *Proc. IEEE Wireless Commun. Netw. Conf. (WCNC)*, 2015, pp. 534–538.

[39] D. Dixit, K. C. Joshi, and S. Sharma, "Performance of intelligent reconfigurable surface-based wireless communications using QAM signaling," 2020, *arXiv:2010.00519*.

[40] V. Kuhn, *Wireless Communications Over MIMO Channels: Applications to CDMA and Multiple Antenna Systems*. Hoboken, NJ, USA: Wiley, 2006.

[41] A. Younis, N. Abuzgaia, R. Mesleh, and H. Haas, "Quadrature spatial modulation for 5G outdoor millimeter–wave communications: Capacity analysis," *IEEE Trans. Wireless Commun.*, vol. 16, no. 5, pp. 2882–2890, May 2017.

[42] D. Tse and P. Viswanath, *Fundamentals of Wireless Communication*. Cambridge, U.K.: Cambridge Univ. Press, 2005.